



Article

Regional GNSS-Derived SPCI: Verification and Improvement in Yunnan, China

Xiongwei Ma ¹, Yibin Yao ^{1,*} and Qingzhi Zhao ^{2,3}

¹ School of Geodesy and Geomatics, Wuhan University, Wuhan 430072, China; xiongw_ma@whu.edu.cn

² College of Geomatics, Xi'an University of Science and Technology, Xi'an 710054, China; zhaoqingzhia@xust.edu.cn

³ Guangxi Key Laboratory of Spatial Information and Geomatics, Guilin University of Technology, Guilin 541000, China

* Correspondence: ybyao@whu.edu.cn

Abstract: From the aspect of global drought monitoring, improving the regional drought monitoring method is becoming increasingly important for the sustainable development of regional agriculture and the economy. The standardized precipitation conversion index (SPCI) calculated by the Global Navigation Satellite System (GNSS) observation is a new means for drought monitoring that has the advantages of simple calculation and real-time monitoring. However, only SPCI with a 12-month scale has been verified on a global scale, while its capability and applicability for monitoring drought at a short time scale in regional areas have never been investigated. Therefore, this study aims to evaluate the performance of SPCI at other time scales in Yunnan, China, and propose an improved method for SPCI. The data of six GNSS stations were selected to calculate SPCI; the standardized precipitation evapotranspiration index (SPEI) and composite meteorological drought index (CI) are introduced to evaluate the SPCI at a short time scale in Yunnan Province. In addition, a modified CI (MCI) was proposed to calibrate the SPCI because of its large bias in Yunnan. Experimental results show that (1) SPCI exhibits better agreement with CI in Yunnan Province when compared to SPEI; (2) the capability of SPCI for drought monitoring is superior to that of SPEI in Yunnan; and (3) the improved SPCI is more suitable for drought monitoring in Yunnan, with a relative bias of 5.43% when compared to the MCI. These results provide a new means for regional drought monitoring in Yunnan, which is significant for dealing with drought disasters and formulating related disaster prevention and mitigation policies.

Keywords: drought; SPCI; precipitable water vapor; CI



Citation: Ma, X.; Yao, Y.; Zhao, Q. Regional GNSS-Derived SPCI: Verification and Improvement in Yunnan, China. *Remote Sens.* **2021**, *13*, 1918. <https://doi.org/10.3390/rs13101918>

Academic Editor: Yuei-An Liou

Received: 27 March 2021

Accepted: 11 May 2021

Published: 14 May 2021

Publisher's Note: MDPI stays neutral with regard to jurisdictional claims in published maps and institutional affiliations.



Copyright: © 2021 by the authors. Licensee MDPI, Basel, Switzerland. This article is an open access article distributed under the terms and conditions of the Creative Commons Attribution (CC BY) license (<https://creativecommons.org/licenses/by/4.0/>).

1. Introduction

Drought has a significant scope of impact on agriculture, society, economy, and ecosystem health [1,2]; therefore, drought forecasting is important for early drought monitoring and warning. In recent years, with the continuous warming of the global climate, extreme drought events occurred frequently. From 1960 to 2016, the annual economic losses caused by drought were estimated to reach \$221 billion [3]. China is particularly affected by long-term drought disasters and has suffered huge social and economic losses in recent decades [4,5]. Many studies have developed drought monitoring models based on hydrology [6], meteorology [7,8], economy [9], agriculture [10] and other aspects [11,12] to quantitatively describe the impact of drought occurrence frequency, duration, and drought intensity [13].

Drought monitoring has been performed from a single precipitation indicator to a comprehensive indicator combined with multiple meteorological factors and then to the monitoring model developed for a specific drought problem [14]. In the past few decades, a series of meteorological drought indexes have been developed, including the Palmer drought severity index (PDSI) [7], self-calibrating PDSI (ScPDSI) [15], standardized

precipitation index (SPI) [16], and standardized precipitation and evapotranspiration index (SPEI) [8]. The above drought indexes have their advantages, but some defects also exist, such as the wide application of SPI; the application of SPI in semi-arid and arid areas is often limited to precipitation, while ignoring the temperature affecting drought [17]; PDSI and ScPDSI comprehensively consider factors such as precipitation, temperature, surface runoff, soil water loss, and supply but exhibit notable problems, such as fixed time scale, poor performance on ice and snow surfaces, and limited spatial comparability [8,18,19]; Vicente-Serrano et al. [8] proposed the SPEI by comprehensively considering precipitation and temperature. This index considers the advantages of SPI and PDSI and can be used to evaluate drought at different time scales and is widely used in global drought research. However, evapotranspiration calculation requires many parameters, which are not easy to obtain in many regions of the world [20]. In 2006, the China Meteorological Administration (CMA) released the comprehensive meteorological drought index (CI), which considers water or heat balance processes and reflects the cause, degree, start, end, and duration of a drought event. This index primarily includes the frequency and duration of the drought. The data involved are easy to obtain, and the physical mechanism is clear, which is convenient for in-depth evaluation of drought occurrence. However, analyses using these data are only applicable to China [21–23].

GNSS meteorology includes the technology and application of retrieving atmospheric elements using the delay caused by GNSS signals passing through the earth's atmosphere [24,25]. Bevis et al. [24] first used GNSS observation to estimate precipitable water vapor (PWV). With the continuous development of GNSS meteorology, the root mean square (RMS) of GNSS-derived PWV is about 1–2 mm, and some studies have applied this value to monitor drought [26–30]. GNSS can obtain PWV with high precision and high spatial-temporal resolution [31], which provides a new means for meteorological disaster monitoring. Bordi et al. [26] found that the precipitation efficiency (PE) based on GNSS-derived PWV is positively correlated with SPI, and GNSS-derived PWV has great potential for drought monitoring, and Jiang et al. [27] proved that drought in Yunnan Province of China could be detected according to the abnormal trend of PWV and vertical critical deformation. Wang et al. [28] found that the nonlinear trend of PWV can be used to monitor drought and flood disasters in Australia, and Zhao et al. [29] optimized the potential evapotranspiration in the process of SPEI calculation based on GNSS-derived PWV and temperature, which effectively improved the monitoring accuracy of SPEI. Zhao et al. [30] proposed a drought index that only used GNSS-derived PWV and precipitation and named it multi-time scale standardized precipitation conversion index (SPCI). This index is in good agreement with the traditional commonly used drought indices, such as the SPEI, at 12- and 24-month scales.

To verify the capacity of SPEI for drought monitoring at different time scales in China, this study considers Yunnan Province as the study area. The SPCI calculated based on PWV and precipitation retrieved from the Crustal Movement Observation Network of China (CMONOC) stations was first obtained; then, the SPEI was calculated using the meteorological data and the CI (GB/T 20481—2006) was determined to analyze and verify the applicability of SPCI on a short time scale in Yunnan. Finally, a calibrated method for SPCI is proposed based on the monitoring deviation of SPCI and CI in Yunnan, China. The error adjustment coefficient was calculated to ensure the accuracy of GNSS-derived SPCI for drought monitoring at any time scale. This method can expand GNSS applications in drought monitoring and has significant applicability for drought monitoring in Yunnan.

2. Data and Methods

2.1. Study Area

Yunnan Province is located on the southwest border of China (21°8′–29°15′N, 97°31′–106°11′E). The terrain is high in the northwest and low in the southeast, gradually decreasing from north to south in a staircase shape (Figure 1). The climate types of Yunnan Province are rich and diverse. Due to the influence of monsoons and complex terrain, the precipitation in this

area is spatially uneven from 560 to 2300 mm. The annual precipitation is approximately 1100 mm, mainly from May to October [32]. Drought is a major problem in the region and is closely related to changes in monsoon and precipitation distribution [33]. Yunnan Province has suffered frequent and severe droughts, especially in central and eastern Yunnan [34,35]. The region also experienced a continuous drought from autumn 2009 to spring 2010 [36,37], resulting in agricultural losses of \$2.5 billion and a lack of drinking water for approximately 9.65 million people [38]. Therefore, this area is ideal for drought monitoring and methodological verification.

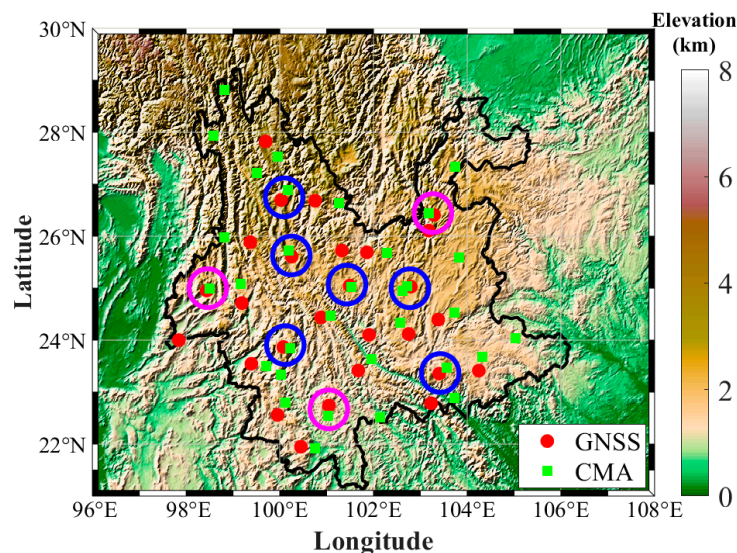


Figure 1. Geographic distribution of GNSS and CMA stations in Yunnan Province. The circle is the collocated station, and the blue circle is used for analysis.

2.2. Data Description

CMONOC is a ground observation infrastructure with a high spatial-temporal resolution, high precision, is multi-scale, in real-time, and compatible with various satellite positioning systems based on the original crustal movement observation network. It is mainly used for crustal deformation monitoring [39], seismic research [40], space environment, and meteorology research [41,42]. In this study, 27 ground-based GNSS stations in Yunnan Province obtained from CMONOC were selected. Among them, nine stations are collocated with the meteorological station (Figure 1) and six of nine stations with long time series are selected for analysis. The GNSS observations sampled at 30 s from March 1999 to April 2015 were processed by the GAMIT/GLOBK software (Ver. 10.4). The cutoff elevation angles were set to 7° and an elevation-dependent weighting strategy was applied to measurements at low elevations (below 30°) to reduce the influence of multipath and the uncertainties in mapping functions at low elevations.

Meteorological data, such as daily maximum temperature, daily minimum temperature, daily average temperature, wind speed, relative humidity, light duration, and precipitation, are provided by the measured dataset of the China Surface Climate Data Daily Dataset (V3.0) of the CMA to calculate the SPEI and CI. The corresponding data from the China Meteorological Forcing Dataset (CMFD) were used to calculate the SPCI. This dataset was generated based on existing international Princeton reanalysis, GLDAS, GEWEX-SRB radiation, and TRMM precipitation data as the background field and was integrated with conventional CMA meteorological observation data. The accuracy of this dataset is dependent on CMA measured data and satellite remote sensing data, which both exhibit higher accuracy than existing international reanalysis data [43]. The specific information of the datasets used in this study is presented in Table 1.

Table 1. Description of datasets used in this study.

Name	Sources	Spatial Coverage	Temporal Resolution	Temporal Coverage	Sources
Temperature max; Temperature min; Wind speed; Relative humidity; Sunshine hours; Precipitation	CMA	826	Daily	1949–2018	http://data.cma.cn/ ; accessed on 12 May 2020
PWV	CMONOC	259	6-hourly	1999–2015	[31]
Precipitation	CMFD	0.1°	Monthly	1979–2018	https://data.tpdc.ac.cn/ ; accessed on 12 May 2020

2.3. Methodology

2.3.1. Correlation Analysis

The Pearson correlation coefficient calculates the linear correlation proposed by Pearson in the 1880s. It is used to measure the linear correlation between two variables and an index reflecting the closeness of the correlation between variables. In this study, the correlation coefficient was used to determine the correlation between the SPCI and CI. The significance level was set at $\alpha = 0.05$. The Pearson coefficient is usually expressed as R , and the value of R is between $[-1, 1]$; the larger the value of $|R|$, the stronger the correlation [44].

2.3.2. Ensemble Empirical Mode Decomposition (EEMD)

The EEMD was proposed by Wu and Huang [45]. This is an improvement in empirical mode decomposition (EMD). The ensemble average of EMD decomposition results was determined to avoid the scale-mixing problem by introducing white noise. This method is suitable for non-stationary and nonlinear signal detection and can gradually separate the oscillation (intrinsic mode function, IMF) or trend components of different time scales from the original signal. In this study, the EEMD algorithm was used to decompose the time series of SPCI, SPEI, and CI to obtain the IMFs of each variable. A significance test was performed for the IMFs of different variables. The signals that pass the significance test are signals with actual physical significance. The eigen components that failed the significance test were removed, and the IMFs that passed the significance test were reconstructed to the new time series. The reconstructed sequence has actual physical meaning and can truly reflect the drought situation; therefore, the applicability of different drought monitoring indices in Yunnan was analyzed by comparing the reconstructed time series of SPCI, SPEI, and CI.

2.3.3. SPCI, CI, and SPEI

(1) SPCI

The SPCI is a new drought monitoring method based on the GNSS-derived PWV and precipitation proposed by Zhao et al. [30]. Bordi et al. [26] found that the precipitation conversion rate based on GNSS-derived PWV can represent regional drought. Therefore, Zhao et al. [30] has added multiple time scales to the traditional precipitation conversion rate calculation and standardized them. The specific calculation process is as follows: first, obtain the PWV and precipitation data of each station and unify these data into the monthly scale; second, add the precipitation and PWV data to the specified monthly scale and calculate the precipitation conversion rate of the specified time scale. The specific expression is as follows:

$$PCI_n = \frac{\sum_{i=m}^{m+n-1} P_i^{total}}{\sum_{i=m}^{m+n-1} PWV_i^{mean} \times day_i} \times 100 \quad (1)$$

where i is the month, P_i^{total} is the total monthly precipitation i , PWV_i^{mean} is the PWV mean of i month, day_i is the number of days of i month, m is the first month of a multi-month scale, n is the total month of a multi-month scale, and PCI_n represents the relative precipitation conversion index of n , the month scale with magnitudes of tens to hundreds. PCI is further standardized owing to its large magnitude, and it is compared with the traditional drought monitoring index:

$$SPCI_n = nor(PCI_n) \quad (2)$$

where nor refers to standardized PCI_n .

(2) SPEI

The SPEI was proposed by Vicente-Serrano et al. [8]. This index combines the sensitivity of the PDSI to the temperature-induced evaporation demand change and the multi-time scale characteristics of SPI. It can identify different drought types under the background of global warming and is widely used to monitor and analyze drought. SPEI can measure drought severity according to intensity and duration and identify the beginning and end of drought events. The SPEI calculation is based on the difference between precipitation and PET, which is standardized. There are many methods to calculate PET, including the Food and Agriculture Organization of the United Nations, which recommended the Penman–Monteith (PM) method as the standard calculation method of evapotranspiration with high accuracy. However, its disadvantage is that the PM method requires many meteorological parameters, which is not easy to obtain in many parts of the world [20,46]. SPEI can be calculated following the formula proposed by Vicente-Serrano et al. [8], where the monthly climatic water balance D_i of month i is initially computed using the difference between precipitation P_i and PET and is expressed as follows:

$$D_i = P_i - PET_i \quad (3)$$

The calculated D_i values are aggregated at different time scales. SPEI is calculated using the three-parameter log-logistic distribution based on the standardized D series. The probability distribution function of the log-logistic distribution for D series can be expressed as

$$F(x) = \left[1 + \left(\frac{\alpha}{x - \gamma} \right)^\beta \right]^{-1} \quad (4)$$

where α , β , and γ are the scale, shape, and origin parameters, respectively, which are obtained using the L-moment procedure [8]:

$$\alpha = \frac{(w_0 - 2w_1)\beta}{\Gamma(1 + 1/\beta)\Gamma(1 - 1/\beta)} \gamma = w_0 - \alpha \Gamma\left(\frac{1 + 1}{\beta}\right) \Gamma\left(\frac{1 - 1}{\beta}\right) \quad (5)$$

where $\Gamma(1 + 1/\beta)$ is the gamma function of $(1 + 1/\beta)$, and w_s is the probability-weighted moments of order s ($s = 0, 1, 2$) and can be calculated as follows:

$$w_s = \frac{1}{n} \sum_{j=1}^n \left(1 - \frac{j - 0.35}{n} \right)^s \quad (6)$$

where n is the number of data points, and j is the range of observations in increasing order. SPEI is then calculated as the standardized values of $F(x)$, as shown as follows:

$$SPEI = W - \frac{2.515517 + 0.802853W + 0.010328W^2}{1 + 1.432788W + 0.189269W^2 + 0.001308W^3} \quad (7)$$

where $W = \sqrt{-2\ln(F(x))}$ when $F(x) < 0.5$, and $W = \sqrt{-2\ln(1 - F(x))}$ when $F(x) > 0.5$. SPEI value of 0 represents 50% of the cumulative probability of D series. Table 2 shows the drought classification of the SPEI [8].

Table 2. Categorization of drought/wet grade by SPEI.

Categories	SPEI Values
Extremely dryness	Less than −2
Severe dryness	−1.99 to −1.5
Moderate dryness	−1.49 to −1.0
Near normal	−1.0 to 1.0
Moderate wetness	1.0 to 1.49
Severe wetness	1.5 to 1.99
Extremely wetness	More than 2

(3) CI

The CI considers the cumulative effects of precipitation and evapotranspiration on current droughts. This index has been used in drought monitoring, impact assessment, and early warning systems and services of the National Climate Center and provincial climate centers with good results. Moreover, this index was widely used as a national standard in 2006 [47–50]. The CI is calculated using the time and seasonal scales of the SPI for the current month and the relative humidity index of the recent month, reflecting the climate anomaly of the short (month) and long (season) time scales and reflects the short time scale water deficit. The specific expression is as follows:

$$CI = a \times SPI_1 + b \times SPI_3 + c \times MI_1 \quad (8)$$

where a and b are 0.4, c is 0.8, SPI is the standardized precipitation index that accumulates over time, and the calculation of SPI for a certain time scale needs completed monthly precipitation data. The detailed formula can be referred Zhang et al. [51] MI is the moisture index, which can be calculated as follows:

$$MI_1 = \frac{P - PET}{P} \quad (9)$$

where P is the accumulated precipitation in the corresponding time scale, and PET has accumulated evapotranspiration at the corresponding time scale. To make the results more accurate, the PM formula was used to calculate PET . The PM formula can be seen Zhao et al. [29]. The distribution of CI drought grades is presented in Table 3 [47].

Table 3. Integrated meteorological drought level division.

Grade	Type	Value of C_i	Scope of Drought Effects
1	No drought	$-0.6 < C_i$	Precipitation is normal or higher than in normal years, moist surface, no signs of drought
2	Light drought	$-1.2 < C_i \leq -0.6$	Precipitation is less than normal years, surface air is dry, soil moisture exhibits mild deficiencies
3	Moderate drought	$-1.8 < C_i \leq -1.2$	Precipitation continued below normal years, soil surface is dry, soil water shortage, surfaces of plant leaves exhibit daytime wilting
4	Serious drought	$-2.4 < C_i \leq -1.8$	Soil appear sustained severe lack of moisture, thicker dry soil, wilting plants, dry leaves, and fruit shedding. Serious negative impact on crops and ecological environment, industrial production, and drinking water
5	Special serious drought	$C_i \leq -2.4$	Soil appeared a serious shortage of water for a long time, Surface plants withered or died, causing a serious impact on crops and ecological environment with a greater impact on drinking water and industrial production

2.3.4. Deviation Rate Calculation

The Formula (11) is used to calculate the drought monitoring deviation percentage between SPCI/SPEI and CI. Firstly, the drought occurrence frequencies of SPCI, SPEI, and CI at 6 Co-located stations are calculated based on the following formula, respectively:

$$F_i = \frac{n_i}{N} \quad (10)$$

where i refers to the level of drought, $1 \leq i \leq 5$, 1–5 refers to no drought, light drought, moderate drought, serious drought and special serious drought, respectively. n_i refers to the number of type i droughts. N refers to the number of all drought types. F_i is the frequency of type i drought. Then, the deviation rate of SPCI and SPEI can be obtained by subtracting $F_i(\text{SPCI})$ and $F_i(\text{SPEI})$ from $F_i(\text{CI})$, respectively.

3. Results

3.1. Correlation Analysis of SPCI and SPEI at Different Time Scales

The SPCI was calculated using the GNSS-derived PWV and CMA-derived precipitation at the 1- to 12-month scales. In addition, the SPEI at corresponding time scales was also obtained, and the PET was calculated using the PM model to guarantee the precision of the calculated SPEI. Figure 2 compares SPEI and SPCI at six collocated GNSS and meteorological stations at the 1- to 12-month scales. The correlation between SPCI and SPEI is poor at short time scales, especially at YNCX and YNMZ stations; the correlation coefficient is less than 0.75 at a 1-month scale. With the increase in time scale, the correlation between the two becomes stronger, the correlation coefficient at the 12-month scale was the highest, and the correlation coefficient of some stations reached 0.97.

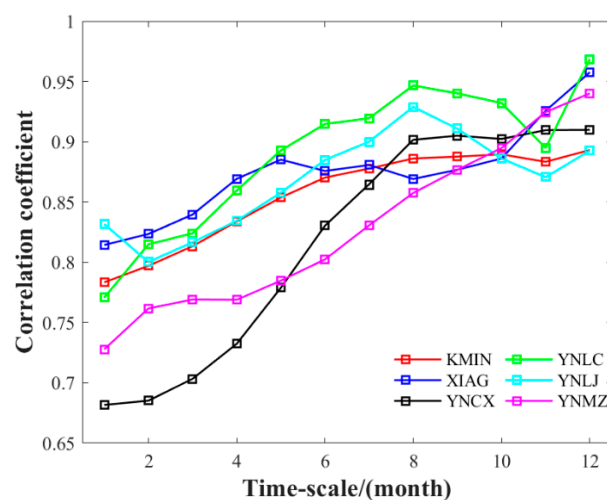


Figure 2. Comparisons of SPEI and SPCI at 6 collocated GNSS and meteorological stations under 1- to 12-month scales.

The physical significance of drought calculation by SPCI and SPEI is different. SPCI that evaluates drought used a ratio between PWV and precipitation [30], while SPEI evaluates drought by subtracting potential surface evapotranspiration from precipitation [8]. Therefore, it is expected that there is a deviation between the two different drought indexes. Both of them can detect drought on the low time scale, but the degree of drought detected is different. With the increase of time scale, the correlation between them increases, which indicates that their drought monitoring effects tend to be the same under the precipitation accumulation. To explore whether SPCI can be used for drought monitoring at a short time scale, this study introduced the CI to verify it at each time scale.

3.2. Correlation Analysis of SPCI/SPEI with CI at Different Time Scales

3.2.1. Determination of Multi-Time Scale CI (MCI)

Due to the multi-time scale characteristics of drought disasters, the superposition of droughts at different time scales may lead to increasingly severe drought. Therefore, it is important to design a multi-time scale CI and expand the application scope and practicability of the CI to analyze drought occurrence and change. According to the CI calculation formula, this study expands the calculation method of CI at the 3-, 6-, and 12-month scales as follows:

$$CI_3 = a \times SPI_3 + b \times SPI_6 + c \times MI_3CI_6 = a \times SPI_6 + b \times SPI_{12} + c \times MI_6CI_{12} = a \times SPI_{12} + b \times SPI_{24} + c \times MI_{12} \quad (11)$$

where CI_3 , CI_6 , and CI_{12} are the CI at the 3-, 6-, and 12-month scales, respectively, and MI is the corresponding accumulated moisture index.

3.2.2. Correlation Analysis of SPCI, SPEI, and CI

Before analyzing the correlation between SPCI and CI, EEMD was first introduced to decompose the SPCI, SPEI, and CI time series. Figure 3 shows the decomposition results for the SPCI. The red line represents the original time series. Lines 2–8 can be divided into six IMFs and the trend term (R). According to the fluctuation characteristics of each IMF component, the frequency of IMF1-IMF6 decreased, the period increased, and the average amplitude decreased. To test the physical significance of IMFs, the IMF energy spectral density period distribution was used to judge the significance of the IMF components [45].

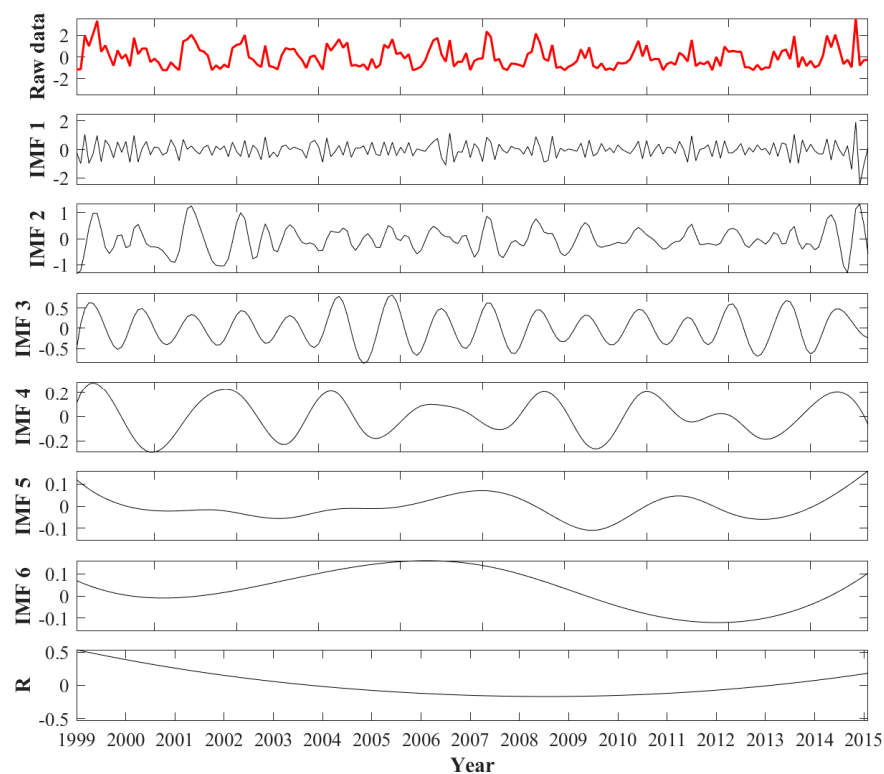


Figure 3. EEMD decomposition of SPCI-01 time series.

Figure 4 shows the significance test of the IMFs of white noise. The IMF component obtained by EEMD decomposition is of practical significance. In this study, $\alpha = 0.05$, 0.01 , and 0.1 are used to obtain the significance test chart of IMF components (Figure 4). The line with a slope of -1 in the figure is the white noise IMF distribution curve. The closer each IMF component is to the line or below the line, the lower is the confidence level of the IMF component. A, B, C, and G are in the 90–99% confidence interval, and the amplitude

is larger than that of the other components. Therefore, the IMF1, IMF2, IMF3, and IMF7 components are more significant, while D, E, and F are close to the white noise line, so they can be considered to have less actual physical significance. In this study, the drought indexes of different time scales were decomposed using EEMD and eliminate the signals that fail to pass the significance test. The SPCI was compared with the commonly used drought indices to test their monitoring performance at each time scale.

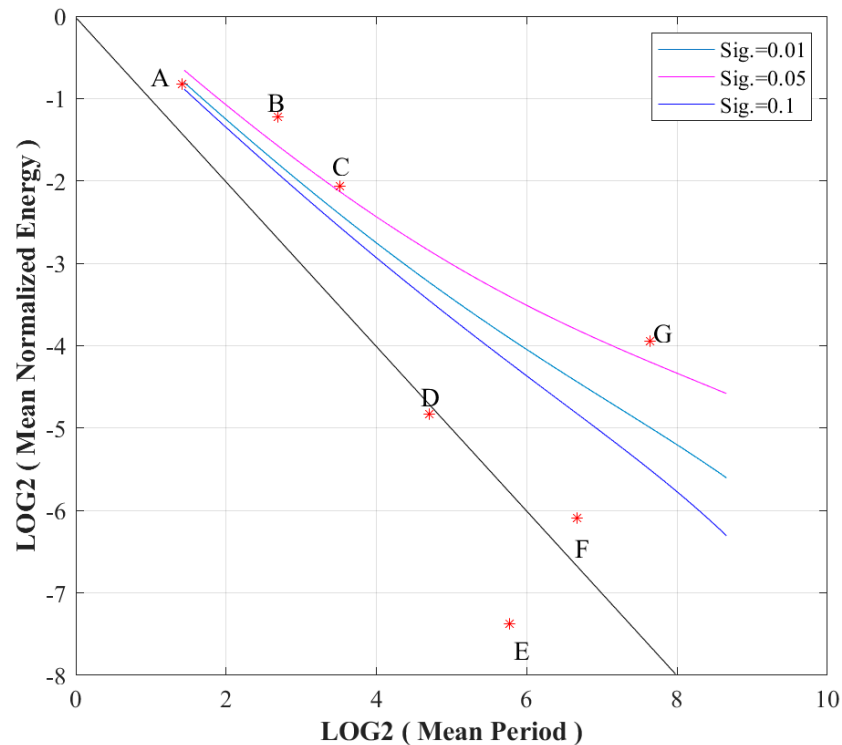


Figure 4. Significance test of IMFs of white noise.

The SPCI, SPEI, and CI time series at a 1-month time scale is first decomposed by EEMD; then, the real intrinsic eigencomponents of different drought index factor time series are obtained and their significance is tested. The eigencomponents that have not passed the significance test are removed, and the remaining IMF components are reconstructed. The results are shown in Figure 5. The long-term variation trend of the three indexes at the KMIN station is relatively consistent and consistent with the change in precipitation. In the case of large precipitation, it is wet, and, in the case of low precipitation, it is dry. By comparing the long-term trend changes of SPEI-01, SPCI-01, and CI-01, it was found that the change trend of SPCI-01 was closer to that of CI-01. In this study, the Pearson method was introduced to calculate the correlation between SPCI and SPEI on the monthly time scale of six stations, and the results are shown in Table 4. Regardless of the original time series or the reconstructed time series after EEMD decomposition, the correlation coefficients of SPEI and CI at the 1-month time scale are less than those of SPCI, and the average correlation coefficients of the original time series and reconstructed time series of the six stations were 0.73/0.90 and 0.75/0.89, respectively. This indicates that the SPCI at the 1-month scale has the potential for drought monitoring in Yunnan.

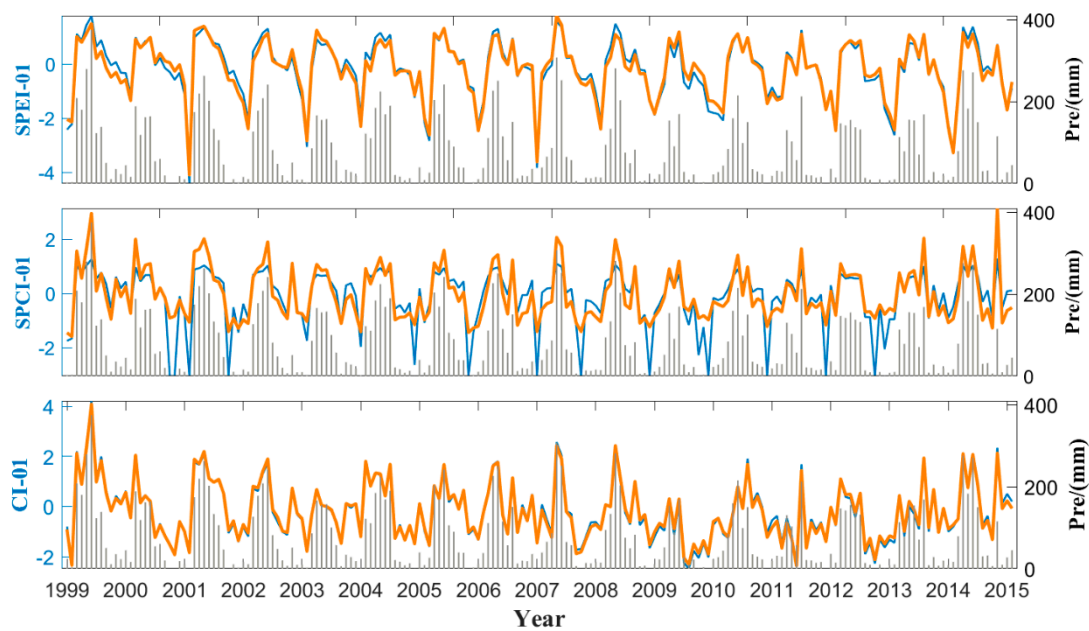


Figure 5. Long-term trend of SPCI-01, CI-01, and SPEI-01 at the KMIN site. Orange lines are signal sequences that pass the significance test.

Table 4. Correlation between CI and SPEI/SPCI-01.

Station Name	Length	SPEI-01		SPCI-01	
		Original	RC	Original	RC
KMIN	1999.03–2015.04	0.71	0.72	0.92	0.92
XIAG	1999.03–2015.04	0.83	0.81	0.92	0.90
YNCX	2010.07–2015.04	0.61	0.62	0.87	0.84
YNLC	2010.08–2015.04	0.72	0.71	0.88	0.86
YNLJ	2010.8–2015.04	0.80	0.77	0.91	0.91
YNMZ	2010.07–2015.04	0.74	0.65	0.88	0.85

Apart from the 1-month scale, the indices at the 3-, 6-, and 12-month scales can represent the drought situation of seasonal, semi-annual, and annual time scales, respectively. In this study, EEMD was used to decompose the drought index of 3-, 6-, and 12-month scales using the same method, and the eigencomponents that pass the significance test were reconstructed. The results are shown in Figure 6. Most eigencomponents decomposed by EEMD of the three indices of the KMIN site can pass the test of significance level of 0.1. Therefore, the reconstructed sequence is slightly different from the original sequence, which indicates that the original sequences of SPCI, SPEI, and CI have physical significance. Figure 6 shows that the trends of SPCI and CI are relatively consistent, but the coincidence of SPEI is relatively poor. The correlation between the original sequence and reconstructed sequence of SPCI and SPEI and the corresponding sequence of CI at all concurrent sites were calculated, and the statistical results are shown in Figure 7. SPCI has a good correlation with CI at all time scales, regardless of whether it is the original sequence or the reconstructed sequence, and the correlation coefficient is greater than 0.8, while SPEI has a poor correlation with CI at the 3- and 6-month scales, and has a strong correlation with CI at the 12-month scale. This indicates that SPCI has the potential to monitor drought at 3-, 6-, and 12-month scales, while SPEI has the potential to monitor drought in Yunnan only at the 12-month scale.

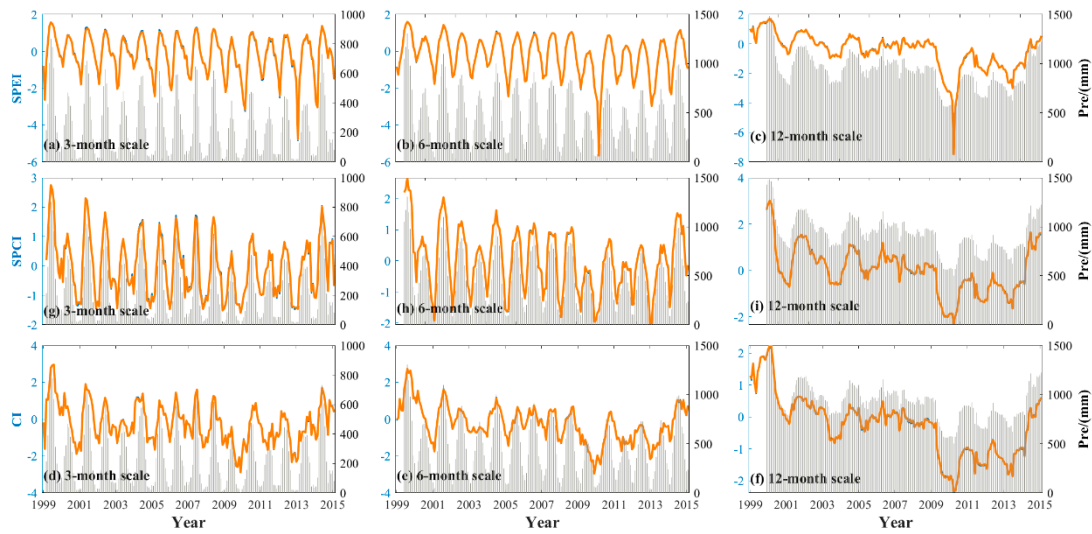


Figure 6. Long-term trends of SPCI, CI, and SPEI in 3-, 6-, and 12-month time scales at KMIN site, respectively. Orange lines are signal sequences that pass the significance test.

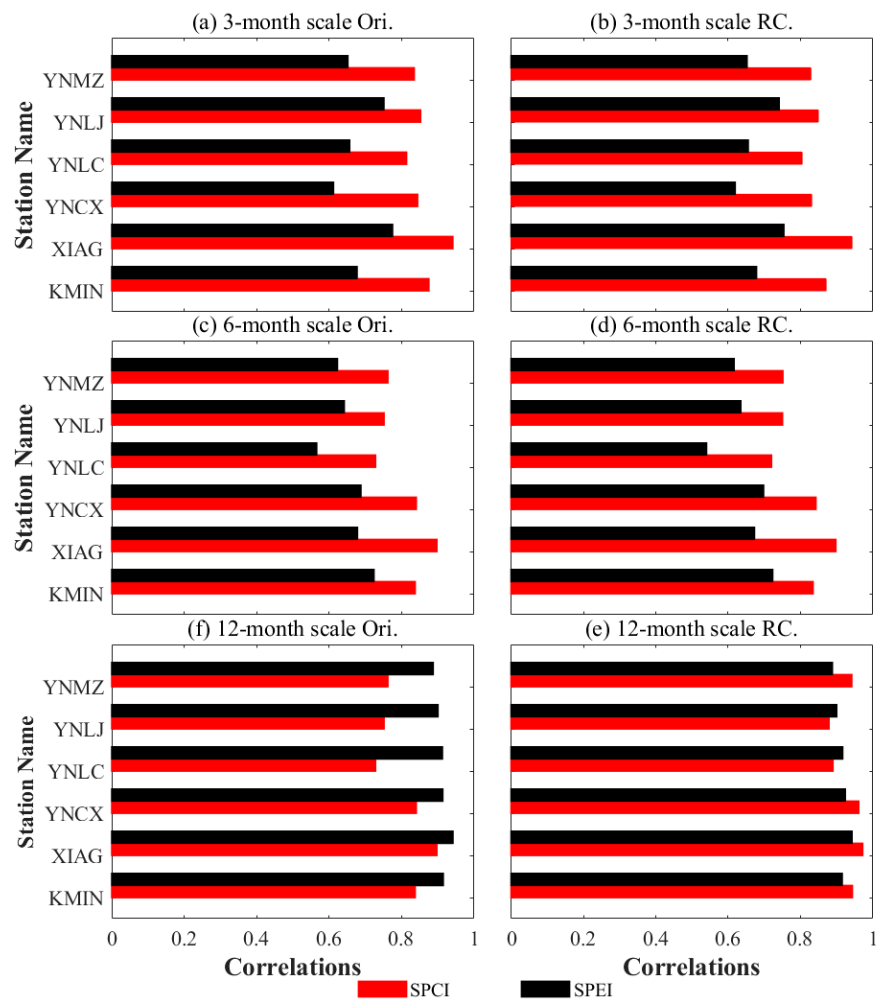


Figure 7. Correlation coefficients between CI and SPEI/SPCI on 3-, 6-, and 12-month scales.

3.3. Comparison of Drought Monitoring Deviation at Different Time Scales

Trend and correlation analysis can only reveal whether they have potential for drought monitoring and cannot be applied to actual drought monitoring. Therefore, this study further verifies the actual drought monitoring ability at six stations. Figure 8 shows the comparison of drought monitoring results of SPCI, SPEI, and CI at monthly, seasonal, semi-annual, and annual time scales. The drought monitoring results of SPCI at different scales are consistent with CI, while the SPEI is relatively poor. In addition, SPEI and SPCI show large deviations in extreme drought disaster monitoring. Because CI has different monitoring standards for different kinds of drought events than those of SPEI and SPCI, the drought monitoring deviations of each index for no, light, moderate, severe, and extreme drought conditions were considered.

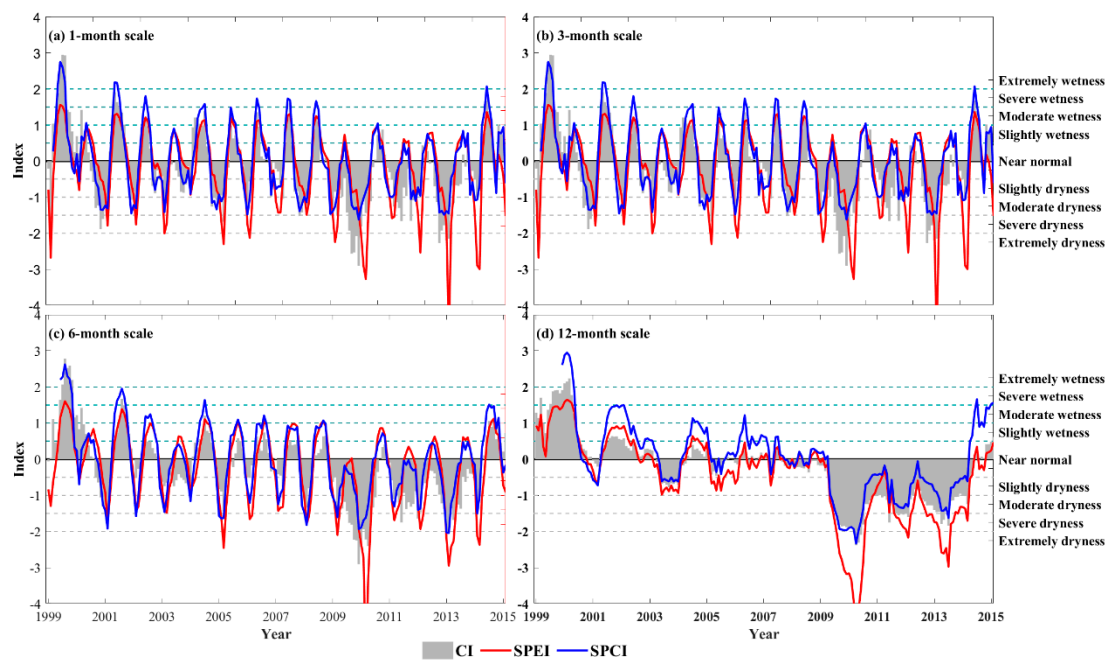


Figure 8. Monitoring deviations of SPCI, SPEI, and CI on 1-, 3-, 6-, and 12-month scales.

Before calculating the monitoring deviation of all drought types, the occurrence frequency of different historical drought types was calculated. As shown in Figure 9, the CI index drought monitoring based on different time scales showed that the frequency of no drought and light drought was high, and the frequency of extreme drought was very low at the time scales of 1, 3, 6, and 12-months. The above statistics and calculations were obtained for SPCI and SPEI, respectively, to further calculate the drought monitoring deviation of the SPCI, SPEI, and CI indices.

The monitoring deviations of SPCI, SPEI, and CI at six sites under four different time scales were counted, and the statistical results shown in Table 5 were obtained. The average deviation of the SPCI for drought monitoring in the 1-, 3-, 6-, and 12-month scales was less than that of SPEI, and the monitoring deviations were 6.77/9.27%, 7.48/9.57%, 8.20/10.32%, and 7.45/9.76, respectively. In different types of drought monitoring, except for extreme drought, the SPCI of other types of drought monitoring was also less than SPEI, which were 3.52/8.31%, 16.76/18.86%, 12.08/15.94%, 4.35/4.86%, and 0.68/0.33%, respectively. The average monitoring deviation between SPCI and CI was 7.48%, which was less than the SPEI (9.73%). These results further prove the suitability of SPCI for drought monitoring in Yunnan.

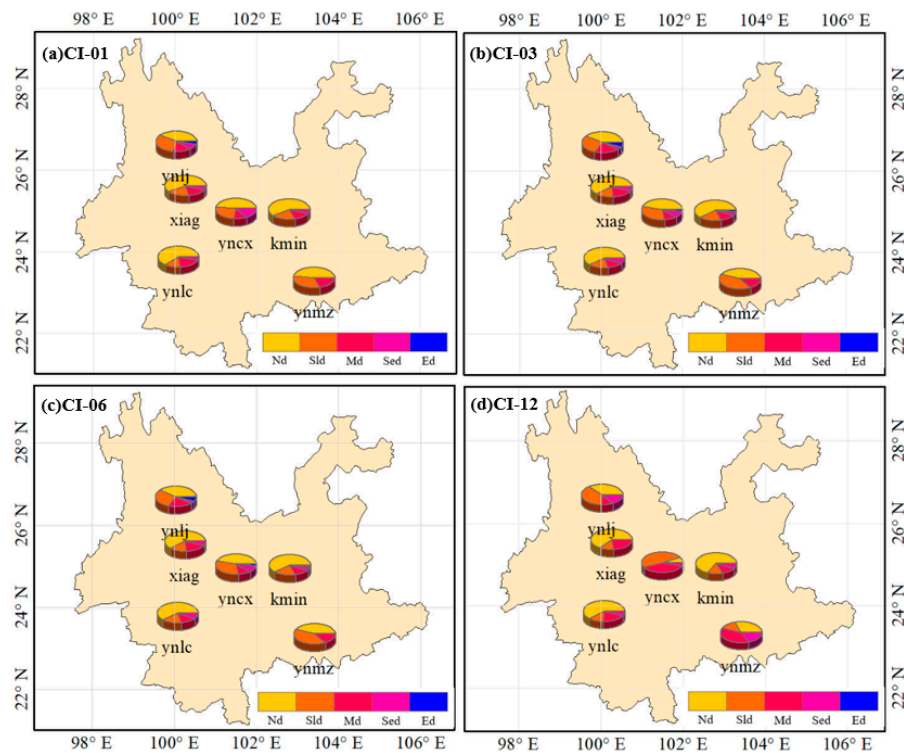


Figure 9. Drought monitoring based on CI.

Figure 10 shows the deviation of SPCI and SPEI for different drought types and CI monitoring results at the 1-, 3-, 6-, and 12-month time scales. SPCI exhibits better performance than SPEI for different kinds of drought monitoring as a whole, and both have a larger deviation from CI monitoring in moderate drought, while SPCI monitoring has a smaller deviation at other time scales. The monitoring deviation of extreme drought is small, mainly because the extreme drought frequency is relatively small in historical drought (Figure 9). Both performed well in drought monitoring, but SPCI was better than SPEI, and the monitoring deviation was less than SPEI at the six stations.

Table 5. Statistical result of monitoring deviation of SPCI, SPEI, and CI at six sites under four different time scales.

	1-Month Scale		3-Month Scale		6-Month Scale		12-Month Scale		Mean	
	SPCI	SPEI	SPCI	SPEI	SPCI	SPEI	SPCI	SPEI	SPCI	SPEI
Nd.	3.41	6.67	6.34	8.80	3.72	9.06	0.60	8.72	3.52	8.31
Sld.	12.40	19.81	16.22	20.82	20.75	20.98	17.69	13.81	16.76	18.86
Md.	11.69	14.51	9.61	13.00	12.90	16.30	14.11	19.93	12.08	15.94
Sed.	5.60	4.96	3.81	4.40	3.10	3.73	4.88	6.33	4.35	4.86
Ed.	0.76	0.38	1.42	0.84	0.55	0.09	0	0	0.68	0.33
Mean	6.77	9.27	7.48	9.57	8.20	10.32	7.45	9.76	7.48	9.73

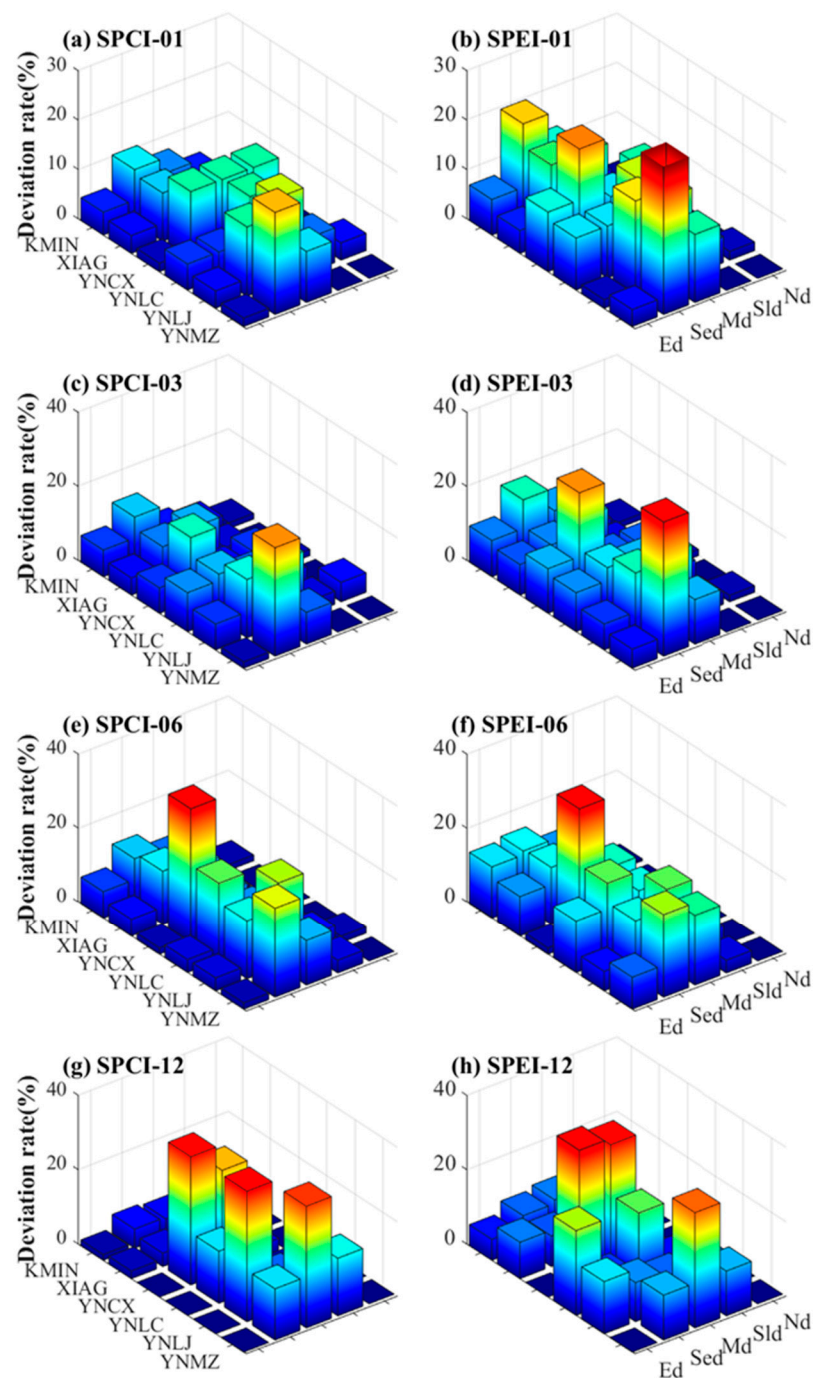


Figure 10. Deviation of different drought monitoring between SPCI, SPEI, and CI, respectively.

4. Discussion

4.1. Different Correlation Coefficients for Different Sites and Scales

Good correlation was observed between SPCI and SPEI; in particular, the 12-month SPCI can be directly applied to drought monitoring [30]. Shi et al. [52] found that, although CRU can obtain global high spatial resolution precipitation data, the data still exhibit obvious errors, especially in mountainous areas [52]. Similarly, the error of the ERA-Interim PWV was 5 mm compared with the measured radiosonde data [53]. Zhao et al. [30] demonstrated that the correlation between SPCI and SPEI at low time scale is relatively poor, especially at the 3- and 6-month scale, and the correlation coefficient is less than 0.6 [30]. However, the correlation between SPCI and SPEI based on the measured data is greater than 0.6, among which the minimum value is 0.68, at the YNCX station, and the

values are greater than 0.73 at other stations, which is better than that of Zhao et al. [30]. The main reason is that the measured data rather than the reanalysis data are used to calculate the SPEI and SPCI in this study, so the results calculated based on the measured data are more accurate. Yunnan's terrain is complex, the regional elevation difference is significant, and the correlations of different stations are different. Overall, the correlation between SPCI and SPEI based on the measured data was higher. If multi-time scale SPCI is used to detect drought, it is suggested that the measured data should be selected instead of the assimilated data. In addition, with the increase in time scale, the effect of drought monitoring under the effect of precipitation accumulation tends to be the same, and the correlation is poor at a short time scale. With the increase in time scale, the correlation increases, which is the same as that of Zhao et al. [30].

4.2. Advantages of EEMD in SPEI Monitoring

The EEMD was introduced and applied to analyze the SPCI, SPEI, and CI. The significant and non-significant signals were separated by a significance test, and the long-term main oscillation series of drought were obtained. Comparing the sequences with practical physical significance to verify the effectiveness of SPCI and SPEI in drought monitoring in Yunnan can highlight whether the SPCI and SPEI are consistent with the actual situation in drought monitoring. The EEMD decomposition of three drought monitoring indices, SPCI, SPEI, and CI, shows that the correlation between SPCI and CI is better than that of SPEI in both the original and reconstructed time series, which confirms the monitoring ability of SPCI. In addition, from Figures 5 and 6, with the increase in time scale, the decomposed non-significant signals decrease, and the original drought index series with a high time scale has practical significance. Therefore, the correlation coefficient between the original and reconstructed signals of SPCI and SPEI in Figure 7 is not obvious. However, the SPEI is lower than that of SPCI, which is more in line with the evolution of drought in the region, while other factors, such as temperature, drive SPEI. In addition, some studies have shown that the SPEI has uncertainty in drought monitoring in Yunnan [54].

4.3. Rationale for Multi-Scale CI

Drought disasters occur along various time scales, and the superposition of different time scales may lead to more serious droughts. Vicente-Serrano et al. [8] pointed out that the drought situation is different under the effect of precipitation accumulation at different time lengths [8], and Paulo et al. [55] also pointed out that the drought indices at the 3-, 6-, and 12-month scales can represent meteorological, agricultural, and hydrological droughts, respectively [55]. Therefore, it is necessary to provide the CI with a multi-time scale designation. The SPCI index has the characteristics of multiple timescales, and the analysis of the practicability of SPCI multi-time scales is of great significance for the promotion of the application scope of the index and the study of drought occurrence. Therefore, according to the CI calculation principle and method, this study designs CI indices of 3-, 6-, and 12-month scales, respectively. The seasonal, semi-annual, and annual time scales of CI can reflect the water change of this quarter/half-year/year and reflect the drought evolution of a longer scale and can profoundly retrieve the drought superposition of different time scales. Some studies have accurately detected Yunnan's drought situation based on the CI index [47]. Therefore, this study can fully evaluate the drought monitoring performance of multi-time scale SPCI with reference to multi-time scale CI.

4.4. Necessity of Calibration

According to the drought classification grades of SPCI, SPEI, and CI, this study monitored different droughts in Yunnan Province. The results showed that the monitoring results of SPCI and CI were in good agreement, while the results of SPEI were in poor agreement. Although the SPEI shows good consistency at the 12-month scale, the performance of SPEI-12 is poor in the actual monitoring application, which indicates that SPEI-12 may not be suitable for characterizing drought conditions under the effect of long-term precipitation

accumulation in Yunnan Province. The authors in [54] also proved this finding. SPCI can monitor drought at any time scale, and the deviation is less than SPEI, but there is still a gap between CI and monitoring results. Therefore, this paper proposes a method to improve the SPCI, and it is found that there is a linear relationship between CI and SPCI and precipitation; the correlation coefficients on 1, 3, 6, and 12-time scales are 0.80, 0.70, 0.63, and 0.94, respectively. Therefore, an improved SPCI (ISPCI) was determined by combining PWV and precipitation.

4.4.1. Improved SPCI (ISPCI) and Validation

Figures 5 and 6 show that there is a close relationship between precipitation and CI. Therefore, this paper proposes an improved SPCI index combined with SPCI and precipitation to monitor drought in Yunnan. ISPCI is expressed as follows:

$$ISPCI = b_0 + b_1 \times \text{nor}\left(\frac{\sum_{i=m}^{m+n-1} P_i^{\text{total}}}{\sum_{i=m}^{m+n-1} PWV_{i,\text{mean}} \times \text{day}_i} \cdot 100\%\right) + b_2 \times \sum_{i=m}^{m+n-1} P_i^{\text{total}} \quad (12)$$

where b_0 , b_1 , and b_2 are estimated by the least-squares method, and the other parameters are the same as in Equations (2) and (3).

Figure 11 shows the deviation between the ISPCI and CI. ISPCI has significantly improved for different types of drought monitoring. According to the deviation in Figure 11, this paper presents the statistical results of the average monitoring deviation of six stations after calibration, as shown in Table 6. It can be found from Table 5 that the SPCI monitoring deviation at the 1-, 3-, 6-, and 12-month scales decreased from 6.77%, 7.48%, 8.20%, and 7.45% to 4.20%, 4.73%, 5.33%, and 7.22%, respectively. In addition, the results shown in the table indicate that the calibrated SPCI exhibited a significant improvement in the monitoring of mild and moderate drought events with an increase from 16.76% and 12.08% to 6.1% and 4.22%, respectively. Considering the four types of time scales of drought monitoring in different degrees, the monitoring deviation of ISPCI in the Yunnan area was found to be reduced from 7.48% to 4.30%, and the improvement rate was 27.41%. This method can effectively improve the drought monitoring accuracy of SPCI in the Yunnan area.

Table 6. Monitoring deviations of different drought between ISPCI and CI (%).

	1-Month Scale	3-Month Scale	6-Month Scale	12-Month Scale	Mean
Nd	4.47	6.64	11.98	10.62	6.72
Sld	5.26	6.62	7.87	10.13	6.10
Md	3.83	44.87	3.10	8.74	4.22
Sed	5.60	4.04	2.59	6.55	3.77
Ed	0.76	1.42	1.12	0.08	0.67
Mean	3.98	4.72	5.33	7.22	4.30

4.4.2. Spatial Comparison of ISPCI and CI in Yunnan

In this section, ISPCI is calculated at 27 GNSS stations in Yunnan Province, and the CI verifies the performance of ISPCI at 32 meteorological stations. Because only six GNSS stations in Yunnan are collocated with meteorological stations, and other non-collocated stations have no precipitation data, this paper introduces the CMFD data, uses the bilinear interpolation method to obtain precipitation at the CMONOC location, and uses CMA-provided precipitation to verify CMFD-provided precipitation. As shown in Figure 12, the scatter diagram shows that CMFD-derived precipitation data has good consistency in this region, and the RMS and bias of the precipitation data are only 5.1 mm and 1.74 mm, respectively. Therefore, the data can be used to calculate ISPCI.

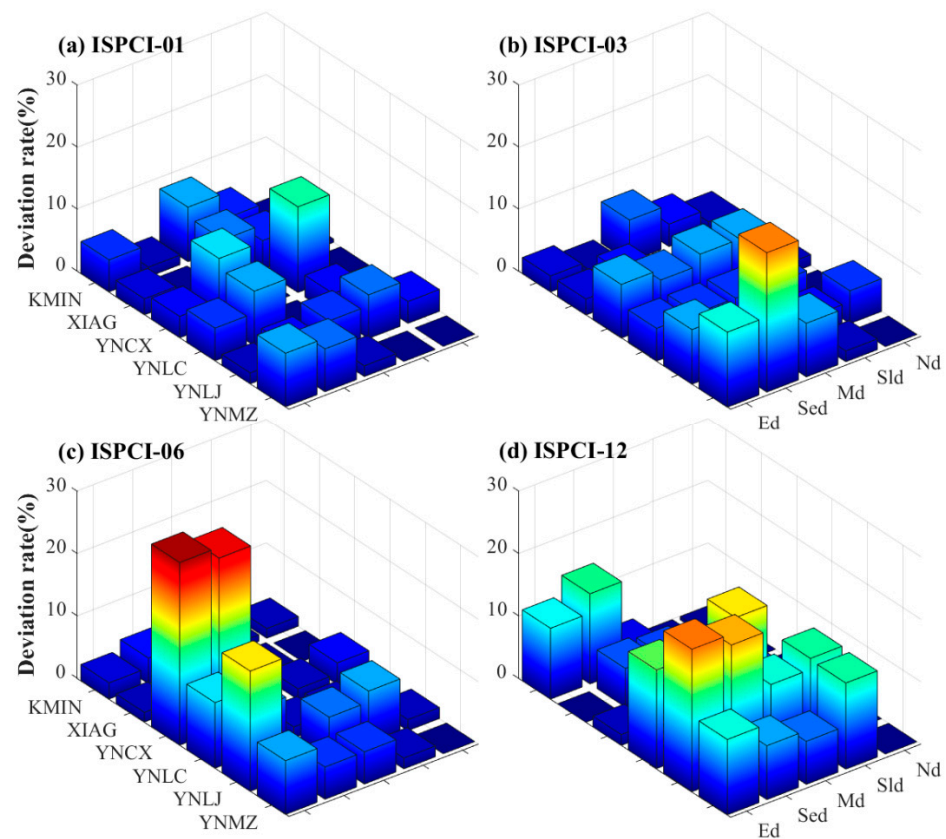


Figure 11. Deviation of different drought monitoring between ISPCI and CI.

The ISPCI of 27 GNSS stations and the CI of 32 meteorological stations in Yunnan were calculated at the time scales of 1, 3, 6, and 12 months. The spatial distributions of ISPCI and CI at different time scales in August 2013 are shown in Figure 13. The drought conditions in Yunnan Province under monthly, seasonal, semi-annual, and annual time accumulation scales are shown in Figure 13a–d. The results indicate that the drought conditions monitored by the two indices were the same. Under the monthly and seasonal time scales, the entire Yunnan region showed no drought; under the half-year time scale, the central and eastern Yunnan showed light drought, and other regions showed no drought; under the cumulative effect of annual precipitation, ISPCI and CI showed moderate to severe drought in central and eastern Yunnan. Both have the same results for drought monitoring in Yunnan at different time scales, which is the same as the research results of [34,35]. Therefore, the proposed ISPCI and CI have the same performance, and ISPCI can be used for actual drought monitoring in this region.

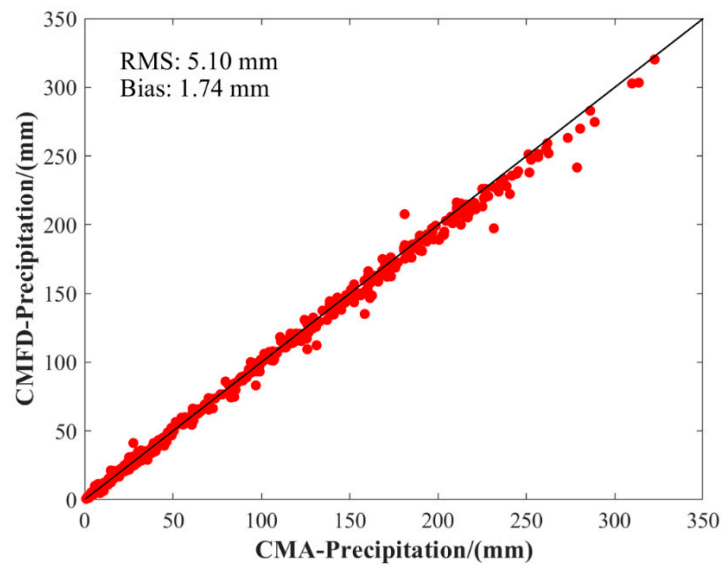


Figure 12. Scatter plots of CMFD-precipitation in the Yunnan.

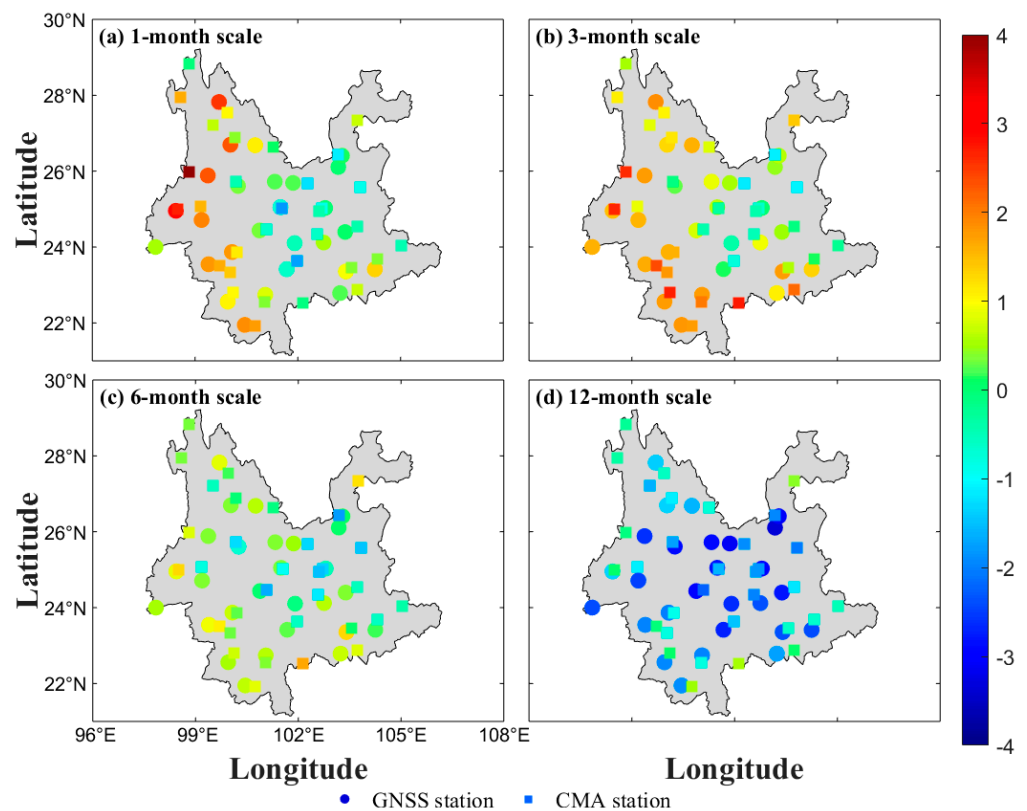


Figure 13. Spatial distribution of ISPCI and CI at (a)1-, (b)3-, (c)6-, and (d)12-month scales in August 2013.

4.5. Limitations and Future Work

Some studies have reported that PWV derived from GNSS plays an important role in extreme natural disasters [31,53,56], particularly in drought and flood disasters [28,57–59]. GNSS-derived SPCI can identify drought and quantitatively evaluate the severity of drought, which is of great significance for drought disaster monitoring. However, GNSS-derived SPCI has only been proven to have good monitoring ability in the global land area at 12- and 24-month scales, and the practicability of drought monitoring at other time

scales is worth further exploration. In this study, the applicability of SPCI at a short time scale was investigated in typical drought-prone areas. It was found that, at the short time scale, SPCI has a strong performance in drought monitoring in Yunnan. Yunnan's terrain is complex, the height difference between the north and south is large, and the number of GNSS stations and meteorological stations is low, which greatly limits the verification of SPCI in Yunnan. In the next step, we will investigate the applicability of SPCI at a short time scale of SPCI in China to expand its application ability. According to the monitoring error of GNSS-derived SPCI in different regions of China, the error adjustment coefficient was constructed to serve the purpose of drought monitoring in China.

5. Conclusions

GNSS-derived SPCI provides a new method for global drought monitoring. The effective use of high-density global GNSS stations can effectively improve the real-time and universality of meteorological drought monitoring. GNSS-derived SPCI has the characteristics of a multi-time scale, which can identify the beginning and end of drought events and measure the severity of drought according to the intensity and duration. To verify the ability of SPCI for drought monitoring, the drought-prone Yunnan area was selected as the research area, and the SPCI, SPEI, and CI at 1-, 3-, 6-, and 12-month scales were calculated using the measured data of six collocated stations from CMONOC and CMA. Based on the CI, it was found that SPCI achieved better drought monitoring accuracy than that of SPEI. Although SPEI has been widely used in drought monitoring and analysis since it was proposed, its applicability in the Yunnan Province of China is worse than that of SPCI. Although SPCI has excellent performance in drought monitoring in Yunnan Province, there is still a deviation between SPCI and CI. After calibrating SPCI, the deviation between ISPCI and CI is smaller. The GNSS-derived SPCI calculation method is simple and can effectively overcome the difficulty of obtaining PM parameters in CI calculations. With the establishment of an increasing number of CORS stations worldwide, GNSS can make significant contributions to global drought disasters, apart from positioning, navigation, and timing.

Author Contributions: Conceptualization, X.M. and Y.Y.; methodology, X.M.; software, X.M.; validation, X.M., Y.Y. and Q.Z.; formal analysis, X.M.; investigation, Q.Z.; resources, Y.Y.; data curation, Q.Z.; writing—original draft preparation, X.M.; writing—review and editing, Q.Z.; visualization, X.M.; supervision, Y.Y.; project administration, Y.Y.; funding acquisition, Y.Y. All authors have read and agreed to the published version of the manuscript.

Funding: This research was funded by the National Natural Science Foundation of China (grant number: 41721003), the Natural Science Basic Research Project of Shaanxi (grant number: 2020JQ-738), and Guangxi Key Laboratory of Spatial Information and Geomatics (grant number: 19-185-10-07).

Institutional Review Board Statement: Not applicable.

Informed Consent Statement: Not applicable.

Data Availability Statement: The data presented in this study are available upon request from the corresponding author.

Acknowledgments: The reviewers' and editors' comments are highly appreciated. We thank Kun Yang from Tsinghua University and Weixing Zhang from Wuhan University for providing the meteorological data and GNSS-derived PWV for this analysis. We would also like to thank the meteorological data providers of the China Meteorological Administration.

Conflicts of Interest: The authors declare that they have no conflict of interest.

References

1. Huang, S.; Huang, Q.; Chang, J.; Leng, G. Linkages between hydrological drought, climate indices and human activities: A case study in the Columbia River basin. *Int. J. Climatol.* **2016**, *36*, 280–290. [[CrossRef](#)]
2. Fang, W.; Huang, S.; Huang, Q.; Huang, G.; Meng, E.; Luan, J. Reference evapotranspiration forecasting based on local meteorological and global climate information screened by partial mutual information. *J. Hydrol.* **2018**, *561*, 764–779. [[CrossRef](#)]
3. Tong, S.; Lai, Q.; Zhang, J.; Bao, Y.; Lusi, A.; Ma, Q.; Li, X.; Zhang, F. Spatiotemporal drought variability on the Mongolian Plateau from 1980–2014 based on the SPEI-PM, intensity analysis and Hurst exponent. *Sci. Total Environ.* **2018**, *615*, 1557–1565. [[CrossRef](#)] [[PubMed](#)]
4. Dai, A. Characteristics and trends in various forms of the Palmer Drought Severity Index during 1900–2008. *J. Geophys. Res. Atmos.* **2011**, *116*. [[CrossRef](#)]
5. Zhang, B.; He, C. A modified water demand estimation method for drought identification over arid and semiarid regions. *Agric. For. Meteorol.* **2016**, *230*, 58–66. [[CrossRef](#)]
6. Shukla, S.; Wood, A.W. Use of a standardized runoff index for characterizing hydrologic drought. *Geophys. Res. Lett.* **2008**, *35*. [[CrossRef](#)]
7. Vicente-Serrano, S.M.; Beguería, S.; López-Moreno, J.I.J. A multiscalar drought index sensitive to global warming: The standardized precipitation evapotranspiration index. *J. Clim.* **2010**, *23*, 1696–1718. [[CrossRef](#)]
8. Palmer, W.C. *Meteorological Drought*; US Department of Commerce, Weather Bureau: Washington, DC, USA, 1965; Volume 30.
9. Reyes-Gomez, V.; Díaz, S.; Brito-Castillo, L.; Núñez-López, D. ENSO drought effects and their impact in the ecology and economy of the state of Chihuahua, Mexico. *Wit Trans. Staten Art Sci. Eng.* **2013**, *64*. [[CrossRef](#)]
10. Sepulcre-Canto, G.; Horion, S.; Singleton, A.; Carrao, H.; Vogt, J. Development of a Combined Drought Indicator to detect agricultural drought in Europe. *Nat. Hazards Earth Syst. Sci.* **2012**, *12*, 3519–3531. [[CrossRef](#)]
11. Esfahanian, E.; Nejadhashemi, A.P.; Abouali, M.; Adhikari, U.; Zhang, Z.; Daneshvar, F.; Herman, M.R. Development and evaluation of a comprehensive drought index. *J. Environ. Manag.* **2017**, *185*, 31–43. [[CrossRef](#)]
12. Rad, A.M.; Ghahraman, B.; Khalili, D.; Ghahremani, Z.; Ardakani, S.A. Integrated meteorological and hydrological drought model: A management tool for proactive water resources planning of semi-arid regions. *Adv. Water Resour.* **2017**, *107*, 336–353. [[CrossRef](#)]
13. Huang, S.; Li, P.; Huang, Q.; Leng, G.; Hou, B.; Ma, L. The propagation from meteorological to hydrological drought and its potential influence factors. *J. Hydrol.* **2017**, *547*, 184–195. [[CrossRef](#)]
14. Ghale, Y.A.G.; Altunkaynak, A.; Unal, A. Investigation anthropogenic impacts and climate factors on drying up of Urmia Lake using water budget and drought analysis. *Water Resour. Manag.* **2018**, *32*, 325–337. [[CrossRef](#)]
15. Wells, N.; Goddard, S.; Hayes, M.J. A self-calibrating Palmer drought severity index. *J. Clim.* **2004**, *17*, 2335–2351. [[CrossRef](#)]
16. McKee, T.B.; Doesken, N.J.; Kleist, J. The relationship of drought frequency and duration to time scales. In Proceedings of the 8th Conference on Applied Climatology, Anaheim, CA, USA, 17–22 January 1993; pp. 179–183.
17. Rousta, I.; Olafsson, H.; Moniruzzaman, M.; Zhang, H.; Liou, Y.-A.; Mushore, T.D.; Gupta, A. Impacts of drought on vegetation assessed by vegetation indices and meteorological factors in Afghanistan. *Remote Sens.* **2020**, *12*, 2433. [[CrossRef](#)]
18. Andreadis, K.M.; Clark, E.A.; Wood, A.W.; Hamlet, A.F.; Lettenmaier, D.P. Twentieth-century drought in the conterminous United States. *J. Hydrometeorol.* **2005**, *6*, 985–1001. [[CrossRef](#)]
19. Wilhite, D.; Pulwarty, R.S. *Drought and Water Crises: Integrating Science, Management, and Policy*; CRC Press: Boca Raton, FL, USA, 2017.
20. Zhang, Q.; Cui, N.; Feng, Y.; Gong, D.; Hu, X. Improvement of Makkink model for reference evapotranspiration estimation using temperature data in Northwest China. *J. Hydrol.* **2018**, *566*, 264–273. [[CrossRef](#)]
21. LI, S.; LIU, R.; SHI, L.; MA, Z.-G. Analysis on Drought tCharacteristic of He’nan in Resent 40 Year Based on MeteorologicalDrought Composite Index. *J. Arid Meteorol.* **2009**, *27*, 97–102.
22. Liu, X.; Li, J.; Lu, Z.; Liu, M.; Xing, W. Dynamic changes of composite drought index in Liaoning Province in recent 50 year. *Chin. J. Ecol.* **2009**, *28*, 938–942.
23. Qian, W.; Shan, X.; Zhu, Y. Ranking regional drought events in China for 1960–2009. *Adv. Atmos. Sci.* **2011**, *28*, 310–321. [[CrossRef](#)]
24. Bevis, M.; Businger, S.; Herring, T.A.; Rocken, C.; Anthes, R.A.; Ware, R.H. GPS meteorology: Remote sensing of atmospheric water vapor using the Global Positioning System. *J. Geophys. Res. Atmos.* **1992**, *97*, 15787–15801. [[CrossRef](#)]
25. Bost, J.; Rohm, W.; Sierny, J.; Kaplan, J. GNSS Meteorology. In *Navigational Systems and Simulators*; CRC Press: Boca Raton, FL, USA, 2011; pp. 79–83.
26. Bordi, I.; Zhu, X.; Fraedrich, K. Precipitable water vapor and its relationship with the Standardized Precipitation Index: Ground-based GPS measurements and reanalysis data. *Theor. Appl. Climatol.* **2016**, *123*, 263–275. [[CrossRef](#)]
27. Jiang, W.; Yuan, P.; Chen, H.; Cai, J.; Li, Z.; Chao, N.; Sneeuw, N. Annual variations of monsoon and drought detected by GPS: A case study in Yunnan, China. *Sci. Rep.* **2017**, *7*, 5874. [[CrossRef](#)] [[PubMed](#)]
28. Wang, X.; Zhang, K.; Wu, S.; Li, Z.; Cheng, Y.; Li, L.; Yuan, H. The correlation between GNSS-derived precipitable water vapor and sea surface temperature and its responses to El Niño–Southern Oscillation. *Remote Sens. Environ.* **2018**, *216*, 1–12. [[CrossRef](#)]
29. Zhao, Q.; Ma, X.; Yao, W.; Liu, Y.; Du, Z.; Yang, P.; Yao, Y. Improved Drought Monitoring Index Using GNSS-Derived Precipitable Water Vapor over the Loess Plateau Area. *Sensors* **2019**, *19*, 5566. [[CrossRef](#)]

30. Zhao, Q.; Ma, X.; Yao, W.; Liu, Y.; Yao, Y. A drought monitoring method based on precipitable water vapor and precipitation. *J. Clim.* **2020**, *33*, 10727–10741. [[CrossRef](#)]
31. Zhang, W.; Lou, Y.; Haase, J.S.; Zhang, R.; Zheng, G.; Huang, J.; Shi, C.; Liu, J. The use of ground-based gps precipitable water measurements over china to assess radiosonde and era-interim moisture trends and errors from 1999 to 2015. *J. Clim.* **2017**, *30*, 7643–7667. [[CrossRef](#)]
32. Duan, X.; Gu, Z.; Li, Y.; Xu, H. The spatiotemporal patterns of rainfall erosivity in Yunnan Province, southwest China: An analysis of empirical orthogonal functions. *Glob. Planet. Chang.* **2016**, *144*, 82–93. [[CrossRef](#)]
33. Zhang, W.; Tang, Y.; Zheng, J.; Cao, J.; Ma, T. Impacts of the vapor transportation by summer monsoon on drought and flooding in summer of Yunnan. *J. Nat. Resour.* **2012**, *27*, 293–301.
34. Peng, G.; Liu, Y.; Zhang, Y. Research on Characteristics of Drought and Climatic Trend in Yunnan Province. *J. Catastrophol.* **2009**, *24*, 40–44.
35. Zhang, W.; Zheng, J.; Ren, J. Climate characteristics of extreme drought events in Yunnan. *J. Catastrophol.* **2013**, *28*, 59–64.
36. Long, D.; Shen, Y.; Sun, A.; Hong, Y.; Longuevergne, L.; Yang, Y.; Li, B.; Chen, L. Drought and flood monitoring for a large karst plateau in Southwest China using extended GRACE data. *Remote Sens. Environ.* **2014**, *155*, 145–160. [[CrossRef](#)]
37. Xu, K.; Yang, D.; Xu, X.; Lei, H. Copula based drought frequency analysis considering the spatio-temporal variability in Southwest China. *J. Hydrol.* **2015**, *527*, 630–640. [[CrossRef](#)]
38. Qiu, J. China drought highlights future climate threats: Yunnan’s worst drought for many years has been exacerbated by destruction of forest cover and a history of poor water management. *Nature* **2010**, *465*, 142–144. [[CrossRef](#)] [[PubMed](#)]
39. Wei, W.; Dijin, W.; Bin, Z.; Yong, H.; Caihong, Z.; Kai, T.; Shaomin, Y. Horizontal crustal deformation in Chinese Mainland analyzed by CMONOC GPS data from 2009–2013. *Geod. Geodyn.* **2014**, *5*, 41–45. [[CrossRef](#)]
40. Liu, R.; Li, H.; Yang, S. Regional crustal deformation characteristic before 2016 Yuncheng M4. 4 earthquake swarm based on CMONOC continuous GPS data. *Geod. Geodyn.* **2016**, *7*, 459–464. [[CrossRef](#)]
41. Shi, H.; Zhang, R.; Nie, Z.; Li, Y.; Chen, Z.; Wang, T. Research on variety characteristics of mainland China troposphere based on CMONOC. *Geod. Geodyn.* **2018**, *9*, 411–417. [[CrossRef](#)]
42. Liou, Y.-A.; Teng, Y.-T.; Van Hove, T.; Liljegren, J.C. Comparison of precipitable water observations in the near tropics by GPS, microwave radiometer, and radiosondes. *J. Appl. Meteorol.* **2001**, *40*, 5–15. [[CrossRef](#)]
43. He, J.; Yang, K.; Tang, W.; Lu, H.; Qin, J.; Chen, Y.; Li, X.J.S.D. The first high-resolution meteorological forcing dataset for land process studies over China. *Sci. Data* **2020**, *7*, 1–11. [[CrossRef](#)]
44. Lee Rodgers, J.; Nicewander, W.A. Thirteen Ways to Look at the Correlation Coefficient. *Am. Stat.* **1988**, *42*, 59–66. [[CrossRef](#)]
45. Wu, Z.; Huang, N.E. Ensemble empirical mode decomposition: A noise-assisted data analysis method. *Adv. Adapt. Data Anal.* **2009**, *1*, 1–41. [[CrossRef](#)]
46. Lang, D.; Zheng, J.; Shi, J.; Liao, F.; Ma, X.; Wang, W.; Chen, X.; Zhang, M.J.W. A comparative study of potential evapotranspiration estimation by eight methods with FAO Penman–Monteith method in southwestern China. *Water* **2017**, *9*, 734. [[CrossRef](#)]
47. Yu, W.; Shao, M.; Ren, M.; Zhou, H.; Jiang, Z.; Li, D. Analysis on spatial and temporal characteristics drought of Yunnan Province. *Acta Ecol. Sin.* **2013**, *33*, 317–324. [[CrossRef](#)]
48. Song, X.; Li, L.; Fu, G.; Li, J.; Zhang, A.; Liu, W.; Zhang, K. Spatial–temporal variations of spring drought based on spring-composite index values for the Songnen Plain, Northeast China. *Theor. Appl. Climatol.* **2014**, *116*, 371–384. [[CrossRef](#)]
49. Song, X.; Song, S.; Sun, W.; Mu, X.; Wang, S.; Li, J.; Li, Y. Recent changes in extreme precipitation and drought over the Songhua River Basin, China, during 1960–2013. *Atmos. Res.* **2015**, *157*, 137–152. [[CrossRef](#)]
50. Shen, R.; Huang, A.; Li, B.; Guo, J. Construction of a drought monitoring model using deep learning based on multi-source remote sensing data. *Int. J. Appl. Earth Obs. Geoinf.* **2019**, *79*, 48–57. [[CrossRef](#)]
51. Zhang, Y.; Li, W.; Chen, Q.; Pu, X.; Xiang, L. Multi-models for SPI drought forecasting in the north of Haihe River Basin, China. *Stoch. Environ. Res. Risk Assess.* **2017**, *31*, 2471–2481. [[CrossRef](#)]
52. Shi, H.; Li, T.; Wei, J. Evaluation of the gridded CRU TS precipitation dataset with the point raingauge records over the Three-River Headwaters Region. *J. Hydrol.* **2017**, *548*, 322–332. [[CrossRef](#)]
53. Zhang, Y.; Cai, C.; Chen, B.; Dai, W. Consistency evaluation of precipitable water vapor derived from ERA5, ERA-Interim, GNSS, and radiosondes over China. *Radio Sci.* **2019**, *54*, 561–571. [[CrossRef](#)]
54. Wang, L.; Zhang, X.; Wang, S.; Salahou, M.K.; Fang, Y. Analysis and Application of Drought Characteristics Based on Theory of Runs and Copulas in Yunnan, Southwest China. *Int. J. Environ. Res. Public Health* **2020**, *17*, 4654. [[CrossRef](#)]
55. Paulo, A.; Rosa, R.; Pereira, L. Climate trends and behaviour of drought indices based on precipitation and evapotranspiration in Portugal. *Nat. Hazards Earth Syst. Sci.* **2012**, *12*, 1481–1491. [[CrossRef](#)]
56. Lee, S.-W.; Kouba, J.; Schutz, B.; Lee, Y.J. Monitoring precipitable water vapor in real-time using global navigation satellite systems. *J. Geod.* **2013**, *87*, 923–934. [[CrossRef](#)]
57. Zhao, Q.; Liu, Y.; Ma, X.; Yao, W.; Yao, Y.; Li, X. An improved rainfall forecasting model based on GNSS observations. *IEEE Trans. Geosci. Remote Sens.* **2020**, *58*, 4891–4900. [[CrossRef](#)]
58. Ma, X.; Zhao, Q.; Yao, Y.; Yao, W. A novel method of retrieving potential ET in China. *J. Hydrol.* **2021**, *598*, 126271. [[CrossRef](#)]
59. Zhao, Q.; Liu, Y.; Yao, W.; Yao, Y. Hourly rainfall forecast model using supervised learning algorithm. *IEEE Trans. Geosci. Remote Sens.* **2021**, 1–9. [[CrossRef](#)]